ACS APPLIED ENERGY MATERIALS

www.acsaem.org Article

Vaper Phase Polymerized PEDOT/Cellulose Paper Composite for Flexible Solid-State Supercapacitor

Boxiao Li, Hendrick Lopez-Beltran, Carrie Siu, Kenneth H. Skorenko, Hui Zhou, William E. Bernier, M. Stanley Whittingham, and Wayne E. Jones, Jr.*

Cite This: https://dx.doi.org/10.1021/acsaem.9b02044 Read Online

ACCESS | Metrics & More | Article Recommendations | Supporting Information

ABSTRACT: A flexible solid-state supercapacitor based on vapor phase polymerized (VPP) PEDOT into cellulose paper matrix (PEDOT/CP) was successfully fabricated. The PEDOT/CP composite material worked as both current collector and electrode in constructed test cells. It had a low sheet resistance of 14 Ω/square and survived the Scotch tape test for adhesion. It also showed excellent stability with no significant conductivity drop after 1000 cycles of bending. The PEDOT from electrode obtained the mass specific capacitance of 179 F/g at scan rate of 10 mV/s, which was among the highest specific capacitances ever reported. This high capacitance was attributed to the combination of the VPP technique and the porous fibrous structure of the cellulose matrix. The EDOT vapor penetrated and polymerized through the CP matrix made of nanometer to micrometer level CP fibers. The highest electrode volumetric capacitance achieved was 13.7 F/cm^3. The whole device achieved an energy density of 0.76 mWh/cm^3 and a power density of 0.01 W/cm^3. Bending the supercapacitor to 90° or rotating to 45° caused no major change in capacitance. Owing to the all nonmetallic materials used to construct the supercapacitor, it can be easily disposed. The incineration of the supercapacitor does not release significant hazardous exhaust.

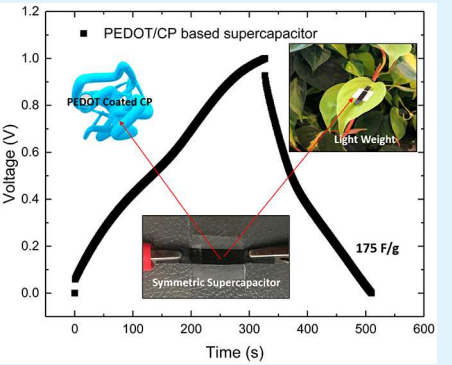

KEYWORDS: *vapor phase polymerization, flexible, supercapacitor, PEDOT, CP matrix, disposable*

1. INTRODUCTION

Supercapacitors have gained much attention due to their high power densities and fast charge times.[1−9] They store much more energy than electrolytic capacitors and charge much faster than batteries.[1] Because of these attributes, the supercapacitor functions as the bridge between battery and electrolytic capacitors. The traditional commercial supercapacitors are inflexible and heavy and cannot be incorporated into wearable applications.[10,11] Flexible and wearable electronics such as displays, circuit structure, sensors, and healthcare devices are becoming more and more attractive to both industrial and academic fields.[12−14] Different flexible displays such as the electronic ink based display with 96 pixels per inch[15] and the MoS_2 thin-film transistor based display[16] have been successfully fabricated. Different kinds of flexible and wearable health monitoring devices such as body temperature sensors,[17] heart rate sensors,[18] and respiration rate sensors[19] have been successfully fabricated. To power flexible lightweight devices in clothing, the development of a robust supercapacitor that can maintain high capacitance under bending and rotating conditions is needed.

Supercapacitors can be divided into two subcategories: electrical double layer capacitors (EDLC) and pseudocapacitors. EDLC stores the charge electrostatically by forming a Helmholtz double layer at the electrode and electrolyte interface.[20−22] This method exhibits fast charge−discharge and stability over thousands of cycles; however, the energy density and capacitance are limited by the available size of electrode and electrolyte interfacial area.[23] EDLC materials such as carbon nanotubes, graphene, and other carbon-based products have been used as electrodes due to their high specific surface area.[24,25] However, issues regarding scale production or large-area processing for these kinds of materials are still unsolved.[25,26]

Pseudocapacitors store charges through redox reactions between electrode and electrolyte. Pseudocapacitors demonstrate high specific capacitance, energy densities, and long cycling life.[27,28] Electrode materials for pseudocapacitors include transition metal oxides,[29] transition metal sulfides,[30] metal nitrides,[31] layered double hydroxides,[32] and conducting polymers.[33] Among different types of electrode materials, only conducting polymers are inherently flexible.

Commonly explored conducting polymers are polyaniline (PANI), polypyrrole (PPy), and poly(3,4-ethylene-

Received: October 16, 2019
Accepted: January 24, 2020
Published: January 24, 2020

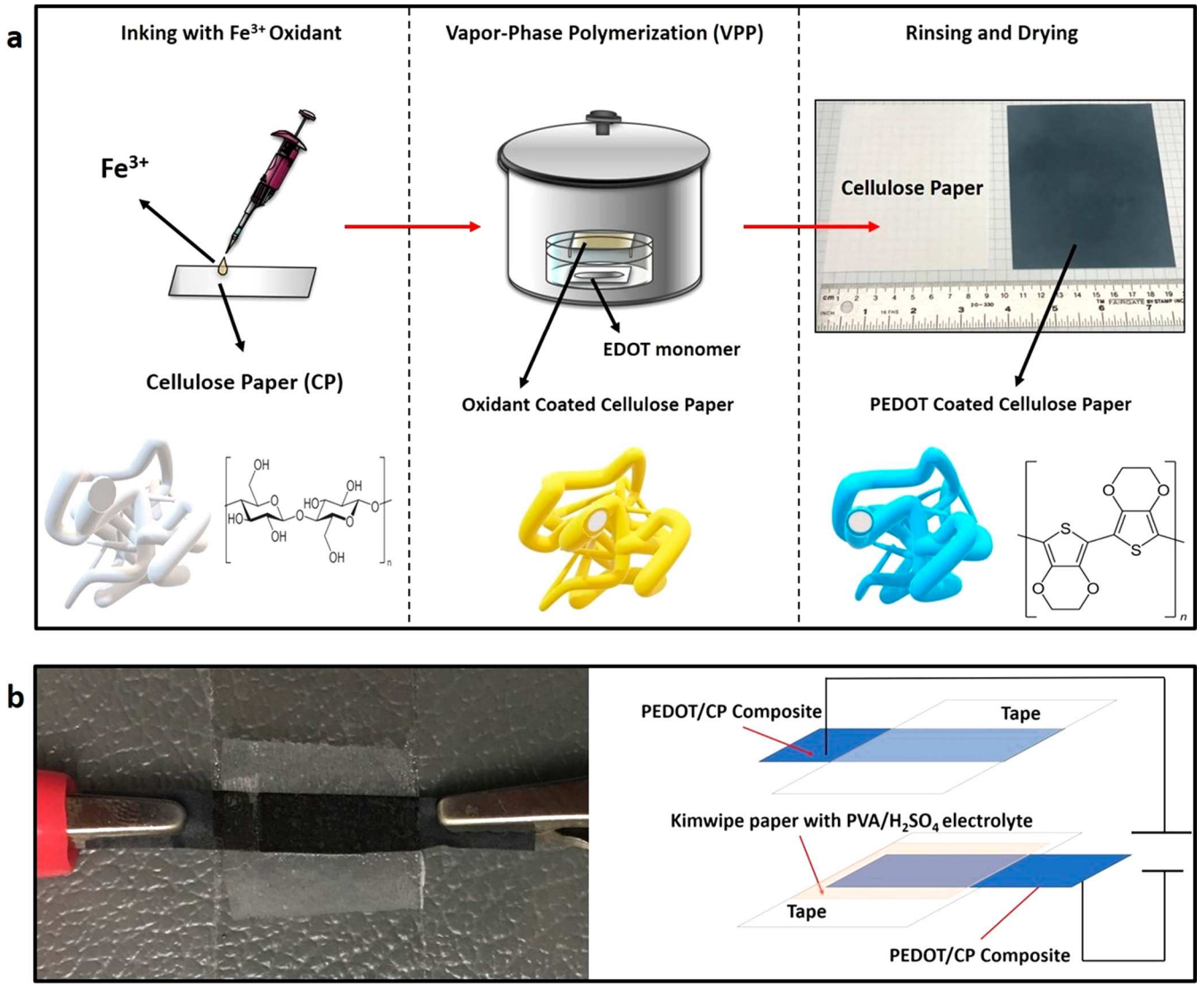

Figure 1. (a) VPP method consisting of inking substrate with oxidant, polymerization, rinsing, and drying alongside a camera image of final product. The bottom row shows their corresponding 3-dimensional depictions. (b) Assembled supercapacitor using PEDOT/CP composite as both electrode and current collector on the left side with its layered structure scheme on the right side.

dioxythiophene) (PEDOT).[34−36] Among these three conducting polymers, PEDOT has received the most attention as a supercapacitor electrode due to its high conductivity of over 1000 S/cm and viability in different processing methods.[37−44]

In previously reported works, many efforts on improving specific capacitance of PEDOT have been exerted. The vapor phase polymerization (VPP) method has been applied to TiO_2 nanorods to generate a VPP-PEDOT/TiO_2 nanocomposite. This nanocomposite achieved a specific capacitance of 87.9 F/g.[3] When VPP was applied to generate VPP-PEDOT with flower-like structure, the specific capacitance achieved was 175 F/g.[45] A PEDOT microsphere with specific capacitance of 160 F/g was synthesized by using the ultrasonic spray polymerization method.[46] In these examples, a noble-metal-based solid current collector or a solid template was used and therefore could not be bent.[3,45,46] A flexible supercapacitor device was achieved by interfacial polymerized PEDOT on cellulose paper (CP) (C_m of 116 F/g); however, the PEDOT synthesized primarily on the surface of the CP, which limited the surface area and capacitance.[47] So far, PEDOT-based supercapacitors rarely demonstrate both flexibility and high mass specific capacitance (C_m) in the same device.

This work details a pathway to synthesize PEDOT/CP composite by using the VPP technique. PEDOT/CP can be fabricated as both current collector and electrode of a highly flexible supercapacitor device. This method results in a robust, lightweight, and disposable composite material with low electrical resistance and high flexibility. This strategy advances the technique by fabricating an inexpensive and flexible PEDOT-based supercapacitor obtaining mass specific capacitance that ranks one of the highest ever reported.

2. EXPERIMENTAL SECTION

2.1. Materials. Iron(III) *p*-toluenesulfonate hexahydrate ($Fe(Tos)_3{\cdot}6H_2O$), iron(III) chloride tetrahydrate ($FeCl_3{\cdot}6H_2O$), 3,4-ethylenedioxythiophene (EDOT) (97%), and poly(vinyl alcohol) (PVA) (MW 85000−124000; 99% hydrolyzed) were purchased from Sigma-Aldrich. Sulfuric acid (H_2SO_4) (~96%), butanol, and pyridine were procured from Fisher Scientific. KimWipes (Science Brand, 4.4 × 8.4 in.^{2}) were purchased from KIMTECH. Cellulose paper (CP) of grade 1 was obtained from Whatman. Ethanol (190 proof) was

https://dx.doi.org/10.1021/acsaem.9b02044
ACS Appl. Energy Mater. XXXX, XXX, XXX−XXX

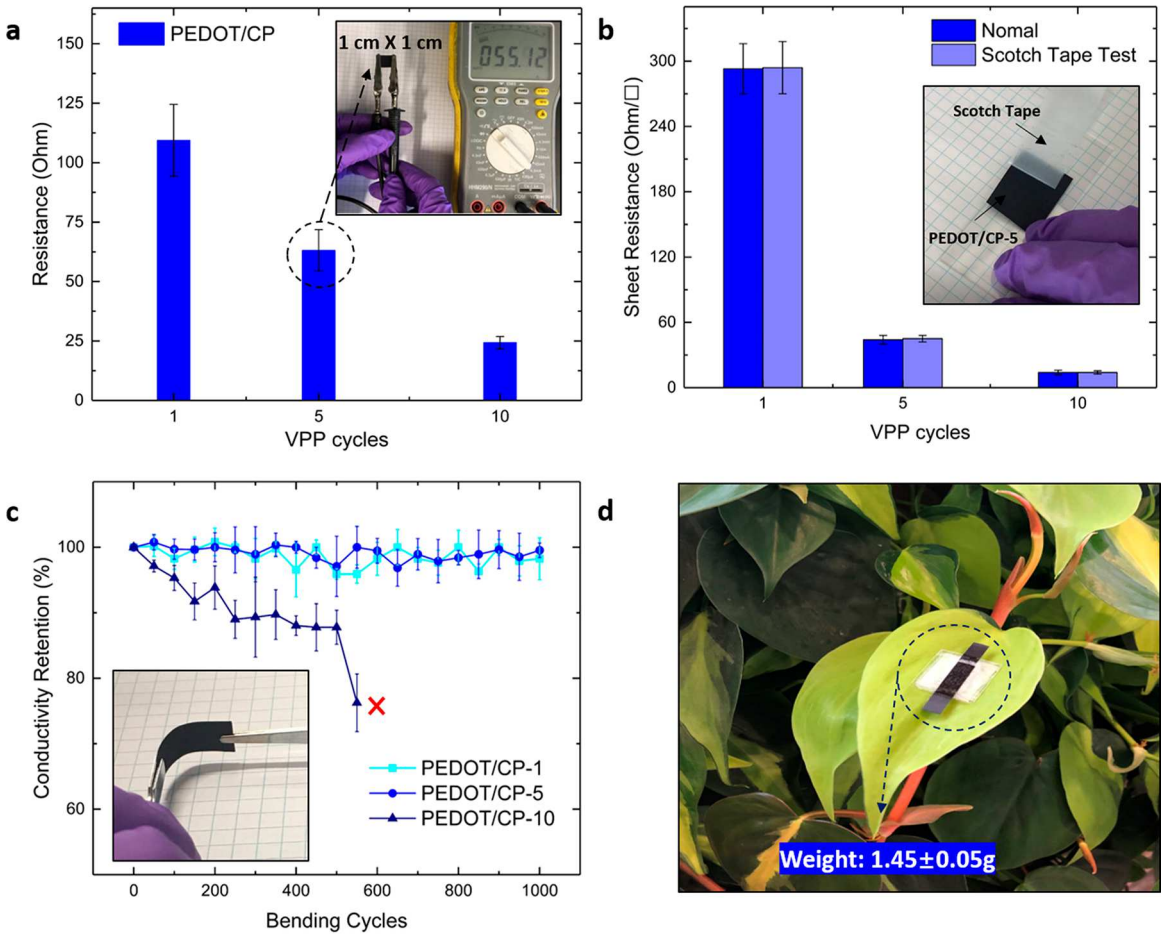

Figure 2. (a) Resistance measurements via the two-probe method on PEDOT/CP composites of different VPP cycles. (b) Sheet resistances of PEDOT/CP composites of different VPP cycles before and after Scotch tape test. (c) Bending cycling test for all the PEDOT/CP materials. (d) Lightweight demonstration for an assembled supercapacitor using PEDOT/CP composite as both electrode and current collector.

acquired from Pharmco-AAPER. All materials were utilized as received.

2.2. Vapor Phase Polymerization. Two different oxidant solutions were prepared. An 8% oxidant solution was prepared by adding 0.8 g of $Fe(Tos)_3 \cdot 6H_2O$ and 80.00 μL of pyridine to 10.00 mL of butanol. The solution was mixed via a sonicator until no solid was observed. An additional solution was prepared by dissolving 0.6 g of $FeCl_3 \cdot 6H_2O$ in 10 mL of methanol. CP was cut into 9 cm by 9 cm sections.

Vapor phase polymerization (VPP) was performed by utilizing a vacuum desiccator from Precision Scientific CO. CP was inked by 2 mL prepared solution and dried on hot plate at 80 °C. 200 μL of EDOT was added to an additional filter paper inside a Petri dish. An 8.5 cm groove across the diameter of Petri dish was created by using two Kapton tape strips placed 8.5 cm apart. Once dry, it was placed atop the groove area, which was above the EDOT-soaked filter paper, and placed into a preheated vacuum desiccator. Water aspiration was activated for 5 min to facilitate polymerization upon the CP. After 5 min, water aspiration was halted, and the sample was set to polymerize for 30 min. This VPP process was repeated on the contrary side of sample to complete one cycle of polymerization. Upon completion of a cycle of polymerization, the sample was rinsed various times with ethanol to remove any remaining oxidant. The sample was dried on hot plate at 50 °C prior to beginning an additional cycle.

2.3. Preparation of PVA-Based Electrolyte. A 10% PVA/H_2SO_4 solution was prepared by dissolving 10 g of PVA into 100.00 mL of 3.0 M H_2SO_4 solution at 80 °C for 4 h with magnetic stirring. The prepared electrolyte solution was cooled before using.

2.4. Construction of Supercapacitor. The PEDOT paper composite was cut into sections of the following dimensions: 0.6 cm wide × 2.5 cm long. Tape was added to each PEDOT section, leaving approximately 1.2−1.3 cm of each electrode's total length exposed in one direction. 10 μL of PVA electrolyte was added and spread by a stick on to the PEDOT paper composite directly under the taped area for each electrode. KimWipe paper was cut into 1.2 cm × 2.0 cm sections. Prior to placing the electrodes together to assemble the supercapacitor, a KimWipe section was added as separator atop of the interface area of a single electrode. An additional 10 μL of PVA electrolyte were added to the surface of the KimWipe to thoroughly ink the separator with electrolyte. Each electrode was finally placed atop another, aligned to have their taped areas to produce an interface area of ~0.75 cm^2.

2.5. Characterization. The morphology and thickness measurement of the PEDOT/CP composite were studied by a Zeiss Supra 55 VP field-emission scanning electron microscope (SEM) at 3 kV. Besides SEM, optical profilometry (Veeco Wyko NT 1100) was also utilized to determine the thickness of each PEDOT/CP composite produced. Raman shift analysis (DXR Smart Raman spectrometer) of the PEDOT/CP composite was performed with a 532 nm excitation laser source. The excitation power applied onto the samples was 3 mW with 2.1 μm spot size. The sample was exposed to laser source 200 times with 0.5 s for each exposure. Raman mapping was performed within 96 μm by 248 μm rectangle area composed of 12 by 31 mapping spots on the cross section of PEDOT/CP composite. Attenuated total reflection Fourier-transform infrared spectroscopy (ATR-FTIR) spectra were collected between 700 and 2000 cm^{-1} by using an IRAffinity-1S spectrometer. The resistances were measured using a two-probe method via a digital multimeter (NEWPORT

https://dx.doi.org/10.1021/acsaem.9b02044
ACS Appl. Energy Mater. XXXX, XXX, XXX−XXX

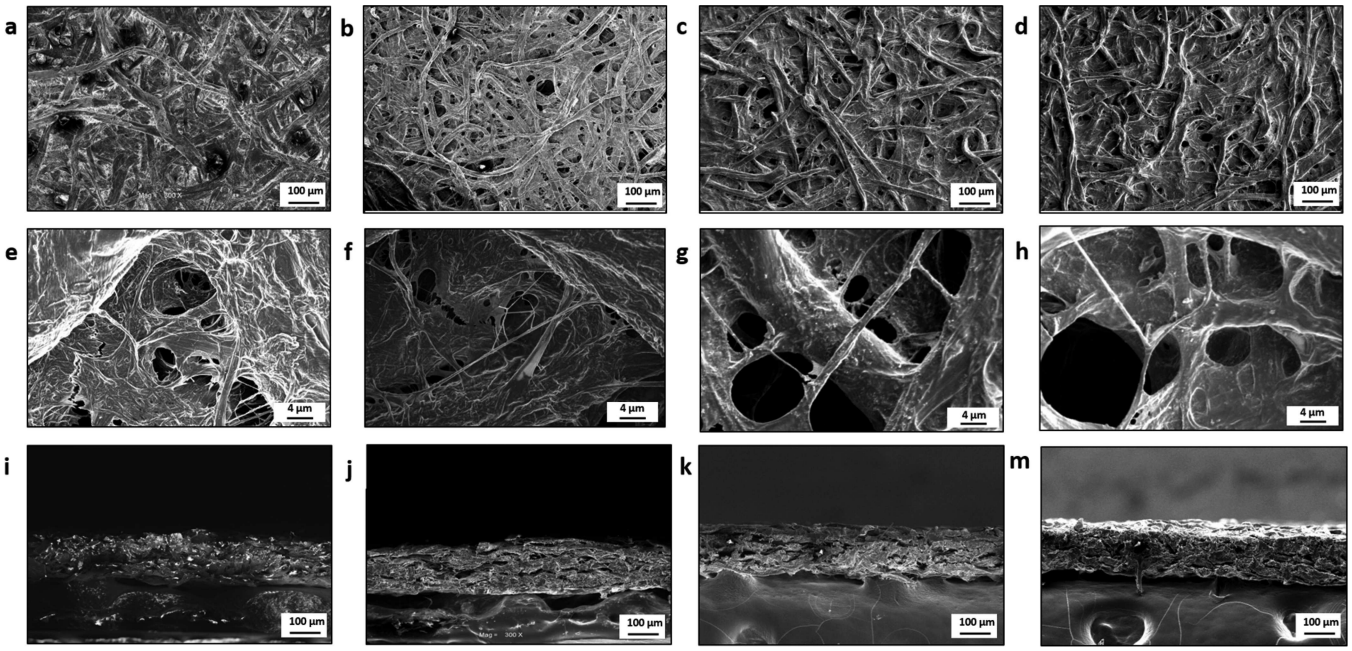

Figure 3. (a–d) From left to right: top views of bare CP, PEDOT/CP-1, PEDOT/CP-5, and PEDOT/CP-10, respectively, at 300× magnification. (e–h) From left to right: top views of bare CP, PEDOT/CP-1, PEDOT/CP-5, and PEDOT/CP-10, respectively, at 6000× magnification. (i–m) From left to right: cross-section views of bare CP, PEDOT/CP-1, PEDOT/CP-5, and PEDOT/CP-10, respectively, at 300× magnification.

HHM290). The sheet resistances of 2.8 cm by 3 cm samples were recorded by a standard four-point probe method. Cyclic voltammetry (CV) profiling, electrochemical impedance spectra (EIS) from 0.01 Hz to 100 kHz, and charging–discharging (CD) test of PEDOT/CP composite were performed by using VMP multichannel potentiostat (Biologic). A CD profile was conducted with a window potential 1.0 V (from 0 to 1.0 V) at varying current flows of current densities. The CV profiling was collected with different scan rate from 10 to 100 mV/s. Thermal analysis was performed on 9.5 mg sample with a TG 209 F1 Iris coupled with a QMS 403 Aeolos mass spectrometer (260-TG/MS Netzsch).

3. RESULTS AND DISCUSSION

3.1. Dual Role of PEDOT/CP Composite.

Figure 1a demonstrates the four steps of VPP method: (1) inking the CP matrix with Fe^{3+} oxidant solution, (2) water-assisted vacuum vapor phase polymerization, (3) rinsing the sample to remove leftover oxidant, and (4) drying of the polymerized CP sample. One VPP cycling discussed in this paper undergoes two VPP processes using the steps described above. The final product of a single cycle of VPP was denoted as a PEDOT/CP-1. PEDOT/CP samples undergoing 5 VPP cycles and 10 VPP cycles were denoted as PEDOT/CP-5 and PEDOT/CP-10, respectively.

Pyridine in the oxidant solution served as the base inhibitor for polymerization. It is believed that the base inhibitor reduced the rate of polymerization and resulted in high conductivity for PEDOT.[38,48] At the beginning of polymerization, water aspiration was adopted to generate a lower pressure and simultaneously introduce water vapor in the VPP chamber for 5 min. It is because that water vapor facilitated the polymerization process and allowed for higher conductivity.[37] A 9 cm by 11 cm sample of blue color was demonstrated (Figure 1a). The resulting mass densities of PEDOT in the samples were 0.4, 0.7, and 1.6 mg/cm^2 for PEDOT/CP-1, PEDOT/CP-5, and PEDOT/CP-10, respectively.

The sandwich structure supercapacitor consisted of two PEDOT/CP electrodes, a PVA/H_2SO_4 electrolyte, a CP separator, and two strips of tape (Figure 1b). The PEDOT/CP composite functioned as both electrode and current collector, separated by a CP separator. The PVA/H_2SO_4 electrolyte was added to the interfaces of both PEDOT/CP electrodes and CP separator prior to the stacking of all components upon each other. Two strips of tape were immediately used to seal the assembled sandwich capacitor to prevent the electrolyte from drying. High electrical conductivity of the PEDOT/CP enabled the material's dual role as electrode and current collector. To demonstrate the performance on electronic conductivity, both resistance and sheet resistance of the material were characterized. As shown in Figure 2a, the resistance of 1 cm by 1 cm samples was measured. PEDOT/CP-1 initially obtained a resistance of 109.4 Ω, PEDOT/CP-5 obtained a resistance of 63.1 Ω, and PEDOT/CP-10 obtained a resistance 24.3 Ω. Therefore, as the VPP cycles increased, the resistance of the PEDOT/CP decreased. Sheet resistances of the sample were recorded by using a four-point probe method as shown in Figure 2b. Observed resistances were 294, 45, and 14 Ω/square for PEDOT/CP-1, PEDOT/CP-5, and PEDOT/CP-10, respectively. It was clear that sheet resistance was reduced significantly upon additional cycles of VPP. Apart from electronic conducting performance, our capacitor design required high adhesion between PEDOT and CP matrix, since the two unprotected ends of PEDOT/CP strips are used to connect with clips (Figure 1b). A Scotch tape test was applied to investigate the adhesion of PEDOT on the CP matrix. As shown in the inset of Figure 2b, upon peeling off the Scotch tape from the PEDOT/CP-5 surface, only small traces of blue color remained on the removed tape, which indicated minimal detachment of PEDOT. Sheet resistances were recorded after the Scotch tape adhesion test to further investigate the detachment of PEDOT/CP. Compared with

https://dx.doi.org/10.1021/acsaem.9b02044
ACS Appl. Energy Mater. XXXX, XXX, XXX–XXX

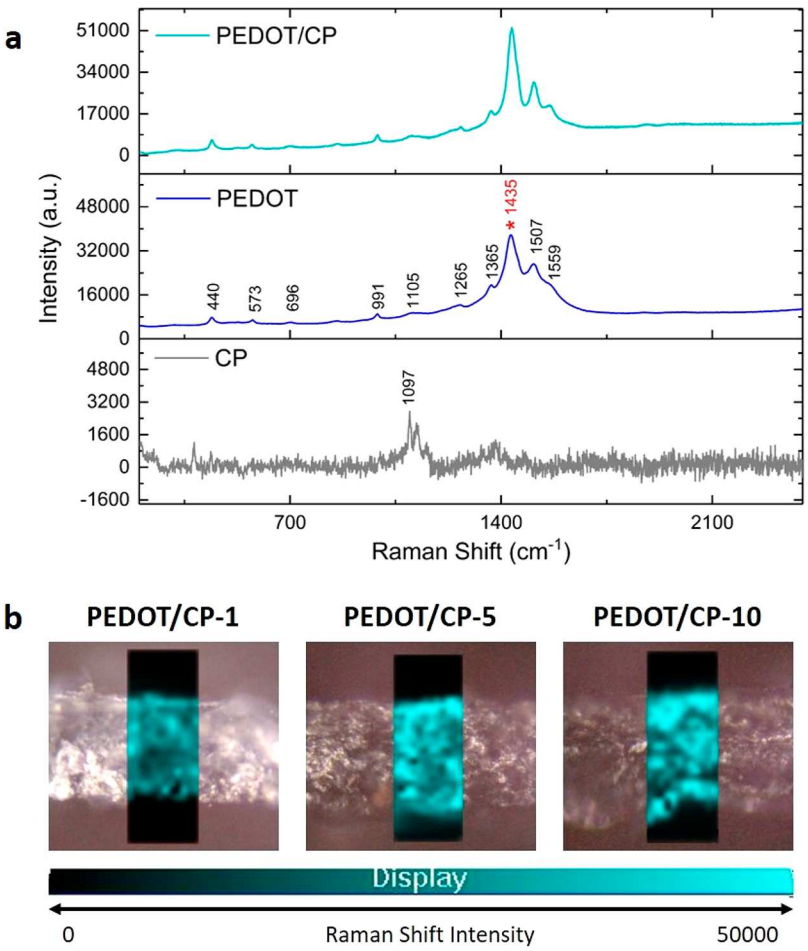

Figure 4. (a) Raman shifts of bare CP matrix (bottom), pure PEDOT (middle), and PEDOT/CP composite (top), where the red star indicates the PEDOT characterization peak used for Raman mapping. (b) Raman mapping results of PEDOT/CP composites of different VPP cycles.

original values, no significant changes were observed in sheet resistance for all PEDOT/CP samples, which suggested adequate adhesion between PEDOT and CP. To render flexibility to supercapacitors, the PEDOT/CP composites needed to be bendable. Therefore, bending tests of PEDOT/CP electrodes were conducted by recording the resistances of the electrode every 50 bending cycles. As resistance is inversely proportional to conductivity, the conductivity retention against bending cycles was plotted as shown in Figure 2c. For each bending cycle, a bending angle of ~90° was reached (inset of Figure 2c). Conductivities of 98.2% and 99.8% were maintained after 1000 cycles of bending for PEDOT/CP-1 and PEDOT/CP-5, respectively. PEDOT/CP-10 demonstrated 88% of the initial conductivity after 500 cycles of bending and tore upon 607 cycles of bending. This suggests that a high mass ratio of PEDOT over CP matrix reduced the flexibility of the PEODT/CP composite. To investigate the influence of the oxidant, the VPP PEDOT/CP composite with $FeCl_3$ as oxidant was synthesized for comparison. PEDOT/CP with $FeCl_3$ oxidant exhibited worse flexibility and lower conductivity than PEDOT/CP with $Fe(Tos)_3$ (Table S1 and Figure S1). To investigate the influence of temperature on the PEDOT/CP sample, a comparative experiment was conducted by setting the VPP chamber at 80 °C. Better flexibility for PEDOT/CP was observed for VPP at 50 °C than VPP at 80 °C (Table S1 and Figure S1).

The high conductivity of the PEDOT/CP composite material enabled a dual role function as both electrode and current collector. The typical assembled simple layered structure (2 of 2.3 cm by 0.6 cm electrodes, a 2.0 cm by 1.2 cm KimWipe separator, and 2 of 1.9 cm by 2.5 cm tapes) PEDOT/CP based supercapacitor obtained the weight of 1.45 g. This lightweight characterization was further demonstrated through placing of the assembled capacitor on a leaf without any visible strain (Figure 2d).

3.2. Morphology and Distribution Analysis. The morphologies of the samples were characterized by SEM. Figures 3a–d present the 300× magnified top views of bare CP, PEDOT/CP-1, PEDOT/CP-5, and PEDOT/CP-10. The porous structures constructed by layered cellulose fibers were observed for all the samples, which indicated that the VPP process, including 10 cycles, did not block the pores on the surface of CP matrix. The diameters of the fibers observed were in the range 10–30 μm. Figures 3e–h present the 6000× magnified top views of bare CP, PEDOT/CP-1, PEDOT/CP-5, and PEDOT/CP-10. Even smaller fibers with diameters at the submicro level were observed for all the samples, which suggested that even 10 cycles of VPP process would not damage the submicro level fibrous structure of the CP matrix. The observed surface roughness decreased from baseline CP as the number VPP cycles increased. This further reduction in roughness indicated that VPP PEDOT coated the cellulose fibers and thus smoothed the surface. Figures 3i–m present the

https://dx.doi.org/10.1021/acsaem.9b02044
ACS Appl. Energy Mater. XXXX, XXX, XXX–XXX

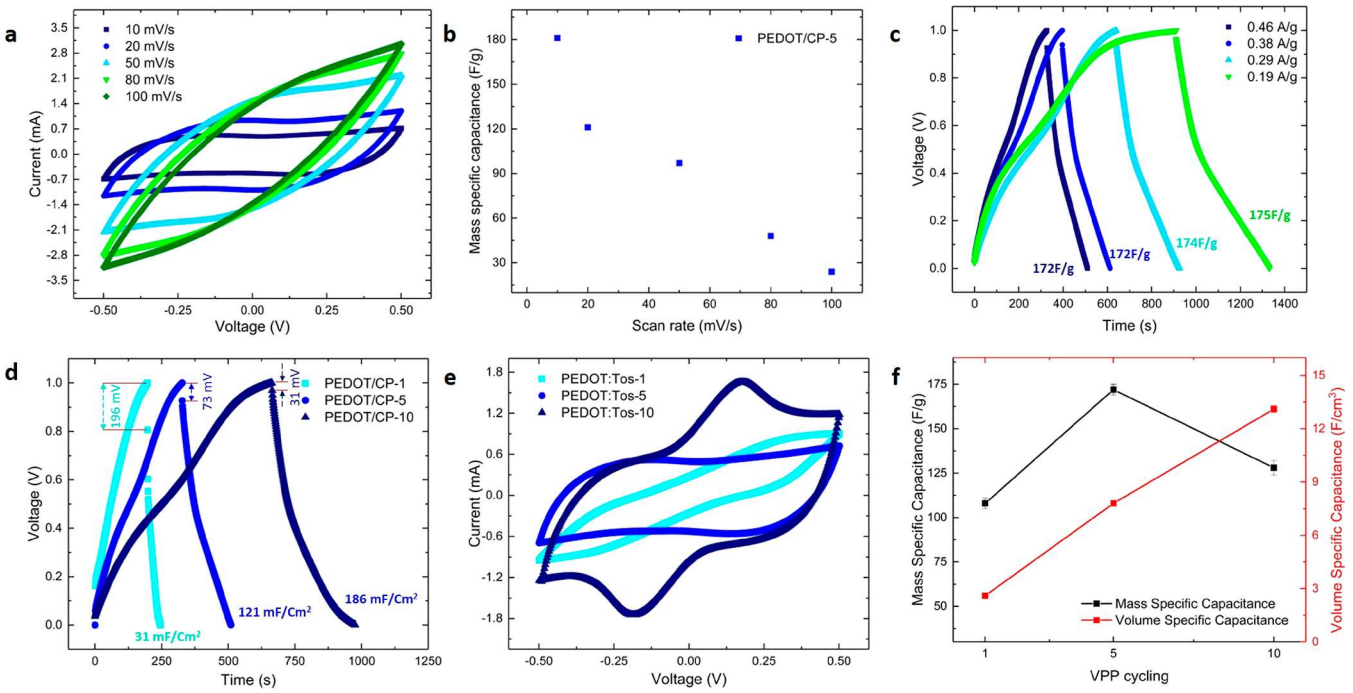

Figure 5. (a) CV profiles of PEDOT/CP-5 supercapacitor with different scan rates. (b) Mass specific capacitances of PEDOT/CP-5 supercapacitor with different scan rates. (c) CD profile of PEDOT/CP-5 supercapacitor with different current densities including 0.19, 0.29, 0.38, and 0.46 A/g. (d) CD profiles of PEDOT/CP supercapacitors constructed by using 1, 5, and 10 VPP cycled composites at a constant current density of 0.32 mA/cm^2. (e) CV profiles at a constant scan rate of 10 mV/s for assembled PEDOT/CP supercapacitor of varying VPP cycles. (f) Calculated mass specific capacitances and volume specific capacitance for PEDOT/CP electrodes of varying VPP cycles based on CD profiles.

300× magnified cross-section views of bare CP, PEDOT/CP-1, PEDOT/CP-5, and PEDOT/CP-10. Their thicknesses were 159 ± 14, 159 ± 17, 160 ± 8, and 155 ± 14 μm, respectively. No significant change in thickness was observed among PEDOT/CP samples. According to previous results, one cycle of VPP process generated a PEDOT thin film with a thickness from tens to hundreds of nanometers.[37−39,48] This suggested that 10 cycles VPP would synthesize PEDOT with the thickness of only hundreds to thousands of nanometers, which was even smaller than the surface roughness of the CP matrix. To further confirm this, the optical profilometry was used to study the thickness of CP and PEDOT/CP-10 samples. As shown in Figure S2, no significant thickness variation was observed.

Because the EDOT monomer was in the vapor phase during the polymerization process and the porous structure of CP matrix was maintained, the hypothesis is that PEDOT formed within and was uniformly distributed throughout the matrix. To demonstrate this, a Raman mapping technique was applied to map the PEDOTs chemical signature in the CP. As shown in Figure 4a, the observed shift at 1097 cm^{-1} was attributed to O−C ring stretching of the bare CP matrix.[49] However, other Raman signals were weak and indefinable. To compare with CP through Raman analysis, pure PEDOT was synthesized by using same VPP method on a glass substrate (Figure 4a). The peak at 440 cm^{-1} was attributed to SO_2 bending. Peaks at 991 and 573 cm^{-1} were attributed to oxyethylene ring deformation. The peak observed at 692 cm^{-1} was attributed to symmetry C−S−C deformation, and the peak observed at 1105 cm^{-1} was attributed to C−O−C deformation. The peak at 1265 cm^{-1} was attributed to $C_\alpha-C_\alpha'$ inter-ring stretching, and the peak observed at 1365 cm^{-1} was attributed to $C_\beta-C_\beta$ stretching. The strongest peak at 1435 cm^{-1} was attributed to symmetry $C_\alpha-C_\beta$ stretching. Finally, the peak observed at 1507 cm^{-1} was attributed to asymmetry C═C stretching, and the peak observed at 1559 cm^{-1} was assigned to bipolaronic states.[38,50] For the PEDOT/CP sample, all the peaks were identical to the pure PEDOT (Figure 4a), and no CP peaks were observed. This was because the intensities of Raman shifts of PEDOT were much stronger than those observed from CP. The strongest PEDOT characterization peak at 1435 cm^{-1} was chosen for Raman mapping to gain insight into the distribution of PEDOT within the CP matrix. Shown in Figure 4b from left to right are cut cross sections of PEDOT/CP-1, PEDOT/CP-5, and PEDOT/CP-10, respectively, and the black box shows the Raman mapping area. The marking cyan color corresponds to the presence of PEDOT, and its intensity represents the quantity of PEDOT. For all the PEDOT/CP samples, the cyan color was distributed evenly throughout the cross section of the CP matrix, which indicated that vapor phase monomers (EDOT) diffused into the matrix and polymerized upon contact with the oxidant-coated fibrous CP. By comparing PEDOT/CP-1, PEDOT/CP-5, and PEDOT/CP-10, we observed a darker cyan color on samples that undergone additional cycles of VPP. This suggested that additional VPP cycles increased the amount of PEDOT in the matrix. More importantly, it suggested that the VPP method could take advantage of fibrous structure within the inner space of the 3-dimensional porous matrix. Fourier transform infrared spectroscopy (FTIR), as the complementary technique to Raman, was used for further identification of the CP matrix and composite materials (Figure S3).

3.3. Electrochemical Performances. The symmetric supercapacitors composed of two PEDOT/CP electrodes were tested via a potentiostat. Each electrode was 0.6 cm by 2.5 cm. An area of ∼0.75 cm^2 (0.6 cm by 1.25 cm) of each

https://dx.doi.org/10.1021/acsaem.9b02044
ACS Appl. Energy Mater. XXXX, XXX, XXX−XXX

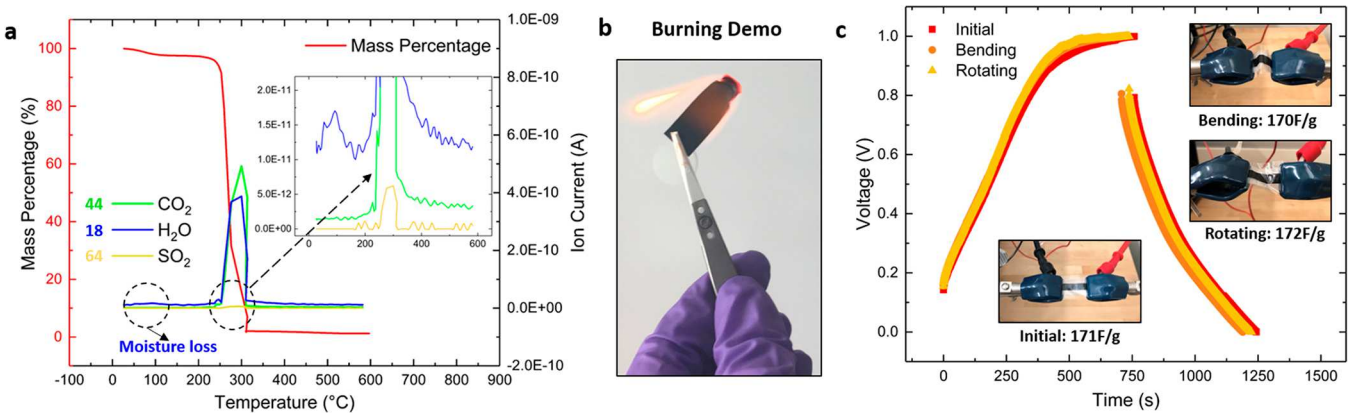

Figure 6. (a) TGA-MS of the PEDOT/CP composite. (b) Burning demonstration using a PEDOT:Tos-5 sample. (c) CV profiles of PEDOT/CP supercapacitor with different conditions including normal, bending, and rotating.

electrode was wet by the electrolyte. Their electrochemical property was characterized by both CV and CD profiles with a potential window of 1 V. The details of all calculations in this section can be found in the Supporting Information. According to Figure 5a, the CV curves of the supercapacitors were plotted for calculating the mass specific capacitance. For example, PEDOT/CP-5 achieved the mass specific capacitance of 179 F/g at scan rate of 10 mV/s. The positive window (0 to 0.5 V) exhibited the same geometry as the negative window (0 to −0.5 V), which indicated the symmetry structure of the supercapacitor (Figure 5a). In this work, the VPP method PEDOT within the CP matrix achieved a C_m of 53% higher than previously reported supercapacitors using interfacial polymerized PEDOT on the top of CP.[47] This suggested that PEDOT using the VPP method can fully take advantage of the high specific surface area of the CP matrix and therefore improved the efficiency of the redox reaction.[45] As the scan rate increased, the capacitance decreased, and 24 F/g was observed at 100 mV/s (Figure 5b). For device performance, the CD profiles were plotted for calculating the specific capacitance of PEDOT. The potential window from 0 to 1 V was selected to achieve high energy density. 1 V is believed to be the potential limit of the PEDOT materials.[51] The CD profiles of the PEDOT/CP-5-based supercapacitor using different charging−discharging current densities from 0.19 to 0.48 A/g were plotted. The mass specific capacitance (C_m) of 172 F/g was achieved based on 0.48 A/g current density, and 175 F/g was achieved based on 0.19 A/g. Within the selected current density range from 0.19 to 0.48 mA/g, no observed significant changes in mass specific capacitances were observed (Figure 5c). The specific capacitance results calculated from CD profiles were 2% smaller than those from CV profiles. This was possibly due to the appearance of irreversible redox reaction when the PEDOT was charged to the potential limit (1 V) in the CD test.[52]

CV profiles for different VPP cycles were compared at the same current density of 0.32 mA/cm^2 as shown in Figure 5d. The calculated area specific capacitances were 37, 121, and 186 mF/cm^2 for PEDOT/CP-1, PEDOT/CP-5, and PEDOT/CP-10, respectively. This can be explained by the increase in the amount of PEDOT per area, which contributes to the capacitance upon additional cycles of VPP. Similarly, the *iR* drops decreased from 196 mV for PEDOT/CP-1 to 73 mV for PEDOT/CP-5 and further to 31 mV for PEDOT/CP-10. Based on the *iR* drops, the equivalent series resistances were 392, 146, and 62 Ω for PEDOT/CP-1, PEDOT/CP-5, and PEDOT/CP-10 devices, respectively. This is due to the increased conductivity from additional cycles of VPP (Figure 2a,b). CV profiles at constant scan rate of 10 mV/s were conducted as shown in Figure 5e, which further confirmed the capacitance change upon increase of VPP cycles. The increase in integrated areas observed upon additional cycles of polymerization from PEDOT/CP-1 to PEDOT/CP-10 indicated higher capacitance. The mass specific capacitance and volume specific capacitance were calculated based on CD profiles. C_m of PEDOT shown in Figure 5f increased from 108 to 172 F/g as the VPP increased from one to five cycles. As the VPP cycles further increased to 10 cycles, C_m dropped to 128 F/g. It is possibly due to the reduction on the specific surface area of the PEDOT, which can be observed by SEM images as discussed previously (Figure 3g,h). The volume specific capacitances (C_v) of the entire electrode, including both PEDOT and CP matrix, increased dramatically as the VPP cycles increased. They were 2.6, 7.9, and 13.7 F/cm^3 for PEDOT/CP-1, PEDOT/CP-5, and PEDOT/CP-10 supercapacitors, respectively (Figure 5f). The significant increase of volume specific capacitance was attributed to the increased amount of PEDOT materials in the CP matrix. For all supercapacitor devices, the volumetric energy densities of the devices (E_v), including two electrodes and a separator, and volumetric power densities (P_v) were calculated based on CD profiles as shown by Figure 5d. As expected, volumetric energy densities were proportional to the cycles of VPP. Energy densities were 0.13, 0.49, and 0.76 mWh/cm^3 for PEDOT/CP-1, PEDOT/CP-5, and PEDOT/CP-10, respectively. Power densities for all the device were around 0.01 W/cm^3.

3.4. Disposability and Flexibility. Cellulose with the chemical formula of $(C_6H_{10}O_5)_n$ is a straight-chain polymer, in which D-glucose is the repeating unit. Cellulose's characterization as biodegradable, regeneratable, nontoxic, flammable, and inexpensive has rendered the organic polymer a disposable and environmentally friendly material.[53,54] Thus, the VPP PEDOT/CP composite material was expected to share these disposable and degradable properties. To gain insight into its disposable property, the TGA-MS technique was employed to examine the exhaust from thermal decomposition. An alumina crucible containing 9.5 mg of PEDOT/CP-5 was put into the chamber under constant O_2 flow. The heating rate was 20 °C/min from 26 to 600 °C. As shown in Figure 6a, from 26 to 100 °C, 2.5% mass loss was attributed to the evaporation of

https://dx.doi.org/10.1021/acsaem.9b02044
ACS Appl. Energy Mater. XXXX, XXX, XXX−XXX

moisture in the PEDOT/CP matrix. The 98.5% mass loss observed from 240 to 320 °C was attributed to the thermal decomposition of both PEDOT and cellulose paper. This temperature range corresponds with previously reported literatures for both PEDOT and CP.[55,56] After 500 °C, 1% of the initial mass remained in the crucible. This is likely due to the insufficient rinsing after VPP, which resulted in a slight amount of remaining impurities such as ferrite ions. To render the material disposable and incinerable properties, exhaust generated upon burning needs to be environmentally friendly. The corresponding mass spectrum suggested three different possible mass products: 44, 18, and 64 g. Based on the chemical composition of the PEDOT/CP composite, the masses were denoted as CO_2, H_2O, and SO_2, respectively. According to Figure 6a, one small band from 26 to 130 °C attributed to the moisture loss. The peaks of all gases overlapped at the same temperature range (from 250 to 330 °C); the mass loss for each emitted component was proportional to integrated area between time (minutes) and ion current (amperes).[57] Compared with CO_2 and H_2O (Figure 6a), SO_2 exhibited a tiny peak as shown in the inset of Figure 6a, which indicated a negligible amount of SO_2 was generated upon burning. As seen in Figure 6b, a burning demonstration of the PEDOT/CP composite was subsequently conducted, which suggested it could be incinerated by the flame. Apart from incineration, a simple recycling process is also favorable. For a traditional supercapacitor, shredding, thermal treatment, fluidized bed separation, and filtration are necessary steps for separating and recycling its parts (including paper, activated carbon, and aluminum foil).[10] On the other hand, because of the paper nature of the PEDOT/CP electrode, it can also be directly disposed in paper recycling bins, since none of the components are environmentally toxic.

The CD cycling ability and flexibility of PEDOT/CP-10 composite electrode were also investigated. The CD cycling ability was tested via a typical assembled supercapacitor. 77% retained capacitance was observed after 1000 charging–discharging cycles (Figure S4a). The Nyquist plots before and after cycling are also shown in Figure S4b.

To demonstrate the flexible property of PEDOT/CP composite, a larger solid supercapacitor device composed of two 2.8 cm by 0.7 cm (length by width) PEDOT/CP-5 electrodes was constructed. It was tested by CD profiles under a constant current of 0.176 A/g at three different conditions: an initial normal state, a 45° rotating state, and a 90° bending state (insets of Figure 6c). The CD profiles of all three three states nearly overlapped with each other. Likewise, the calculated results were 171, 172, and 170 F/g, as shown in Figure 6c. This suggested that 90° bending or 45° rotating did not cause enough strain to fail either the PEDOT/CP electrodes or separator of an assembled supercapacitor.

4. CONCLUSIONS

A PEDOT/CP composite material was successfully produced via the vapor phase polymerization method. As proven by Raman mapping, SEM, and optical profilometry, PEDOT distributes evenly within the CP matrix, and VPP does not cause significant changes on thickness. The PEDOT/CP composites are sufficiently conductive to function as current collectors. Both resistance and sheet resistance decrease as the VPP cycle increases, and a sheet resistance of 14 Ω/square is observed for the 10-cycle VPP sample. Adhesion between PEDOT and CP withstands the Scotch tape test without significant conductivity loss. Similarly, even after 1000 cycles of 90° bending, both PEDOT/CP-1 and PEDOT/CP-5 maintain 98% of their initial conductivity. The PEDOT/CP-10 maintains 90% of the initial conductivity after 500 cycles of bending. A typical assembled supercapacitor exhibits a lightweight of 1.45 g. The PEDOT/CP-5 sample achieved a mass specific capacitance of 179 F/g at a scan rate of 10 mV/s. The electrode volume specific capacitance (C_v) increases dramatically as the VPP cycle increases. PEDOT/CP-1 and PEDOT/CP-10 obtained volume specific capacitance of 4.3 and 13.7 F/cm^3, respectively. This is because the total volume of the electrode is maintained despite the increase in VPP cycles. A point of great interest is that the VPP technique successfully fills the porous CP matrix with conducting polymer and furthermore takes advantage of the high specific surface area of the matrix to enhance the volumetric capacitance.

Although we only produced a 10-cycle VPP PEDOT/CP, the potential for improving the capacitance and power density via additional VPP cycles is promising. The constructed supercapacitor can withstand 90° bending and 45° rotating without compromising capacitance. In addition, our PEDOT/CP supercapacitor retains 77% capacitance after 1000 cycles. According to TGA-MS, abundant amounts of CO_2 and H_2O and a negligible amount of SO_2 were generated upon combustion of the composite, which indicates its environment-friendly property as a disposable material. These results highlight the VPP PEDOT/CP composite as a potential candidate for other flexible conductive applications such as substrates, sensors, or batteries for general electronics.

■ ASSOCIATED CONTENT

Supporting Information

The Supporting Information is available free of charge at https://pubs.acs.org/doi/10.1021/acsaem.9b02044.

All the calculation details, resistances, and sheet resistances (Table S1) for 80 °C-PEDOT/CP-5 and PEDOT:Cl/CP-5, bending cycling test results (Figure S1) for 80 °C-PEDOT/CP-5 and PEDOT:Cl/CP-5, surface and cross-section morphologies of PEDOT/CP-10 electrode and CP matrix (Figure S2) using an optical profilometer, FTIR of the CP matrix and PEDOT/CP sample and charging–discharging cycling stability test with corresponding Nyquist plots of device based on PEDOT/CP-10 electrodes (Figure S4) (PDF)

■ AUTHOR INFORMATION

Corresponding Author

Wayne E. Jones, Jr. − *University of New Hampshire, Durham, New Hampshire 03824, United States;* orcid.org/0000-0002-4519-051X; Email: Wayne.Jones@unh.edu

Authors

Boxiao Li − *Department of Materials Science and Engineering, Binghamton University, Binghamton, New York 13902, United States;* orcid.org/0000-0002-5858-7161

Hendrick Lopez-Beltran − *Department of Electrical Engineering, University of Colorado Denver, Denver, Colorado 80204, United States*

Carrie Siu − *Department of Materials Science and Engineering, Binghamton University, Binghamton, New York 13902, United States*

https://dx.doi.org/10.1021/acsaem.9b02044
ACS Appl. Energy Mater. XXXX, XXX, XXX−XXX

Kenneth H. Skorenko − *ChromaNanoTech, Binghamton University, Binghamton, New York 13902, United States*
Hui Zhou − *Department of Materials Science and Engineering, Binghamton University, Binghamton, New York 13902, United States*
William E. Bernier − *ChromaNanoTech, Binghamton University, Binghamton, New York 13902, United States*
M. Stanley Whittingham − *Department of Materials Science and Engineering, Binghamton University, Binghamton, New York 13902, United States*

Complete contact information is available at: https://pubs.acs.org/10.1021/acsaem.9b02044

Notes

The authors declare no competing financial interest.

■ ACKNOWLEDGMENTS

This work was supported by the National Science Foundation Research Experiences for Undergraduates Program (DMR-1658990). Our thanks go to Dr. Jeffrey Mativetsky for his efforts on organization of the program. B.L., K.H.S., and W.E.B. acknowledge the financial assistance provided by The Strategic Partnership for Industrial Resurgence (SPIR) program (Project no. 990). H.L.-B. acknowledges the financial assistance provided National Science Foundation Research Experiences for Undergraduates Program (DMR-1658990). H.Z. and C.S. acknowledge the financial assistance provided Department of Energy (DOE) through the Advanced Battery Materials Research Program (Battery500 Consortium).

■ REFERENCES

(1) Zuo, W.; Li, R.; Zhou, C.; Li, Y.; Xia, J.; Liu, J. Battery-Supercapacitor Hybrid Devices: Recent Progress and Future Prospects. *Adv. Sci.* **2017**, *4* (7), 1−21.
(2) Zhang, L. L.; Zhao, X. S. Carbon-Based Materials as Supercapacitor Electrodes. *Chem. Soc. Rev.* **2009**, *38* (9), 2520−2531.
(3) Tong, L.; Liu, J.; Boyer, S. M.; Sonnenberg, L. A.; Fox, M. T.; Ji, D.; Feng, J.; Bernier, W. E.; Jones, W. E. Vapor-Phase Polymerized Poly(3,4-Ethylenedioxythiophene) (PEDOT)/TiO_2 Composite Fibers as Electrode Materials for Supercapacitors. *Electrochim. Acta* **2017**, *224*, 133−141.
(4) Shin, D.; Hwang, H.; Yeo, T.; Seo, B.; Choi, W. Thermopower Wave-Driven Hybrid Supercapacitor Charging System. *ACS Appl. Mater. Interfaces* **2016**, *8* (45), 31042−31050.
(5) Liang, Z.; Zhao, R.; Qiu, T.; Zou, R.; Xu, Q. Metal-Organic Framework-Derived Materials for Electrochemical Energy Applications. *EnergyChem.* **2019**, *1* (1), 100001.
(6) Yan, Y.; Luo, Y.; Ma, J.; Li, B.; Xue, H.; Pang, H. Facile Synthesis of Vanadium Metal-Organic Frameworks for High-Performance Supercapacitors. *Small* **2018**, *14* (33), 1−8.
(7) Li, X.; Xiao, X.; Li, Q.; Wei, J.; Xue, H.; Pang, H. Metal (M = Co, Ni) Phosphate Based Materials for High-Performance Supercapacitors. *Inorg. Chem. Front.* **2018**, *5* (1), 11−28.
(8) Yan, Y.; Gu, P.; Zheng, S.; Zheng, M.; Pang, H.; Xue, H. Facile Synthesis of an Accordion-like Ni-MOF Superstructure for High-Performance Flexible Supercapacitors. *J. Mater. Chem. A* **2016**, *4* (48), 19078−19085.
(9) Li, D.; Xu, H.-Q.; Jiao, L.; Jiang, H.-L. Metal-Organic Frameworks for Catalysis: State of the Art, Challenges, and Opportunities. *EnergyChem.* **2019**, *1* (1), 100005.
(10) Jiang, G.; Pickering, S. J. Recycling Supercapacitors Based on Shredding and Mild Thermal Treatment. *Waste Manage.* **2016**, *48*, 465−470.
(11) Janes, A.; Tönurist, K.; Thomberg, T.; Lust, E. Comparison of Electrospun and Commercially Available Separator Materials for Supercapacitors. *ECS Trans.* **2009**, *19*, 23−32.
(12) Singh, E.; Singh, P.; Kim, K. S.; Yeom, G. Y.; Nalwa, H. S. Flexible Molybdenum Disulfide (MoS 2) Atomic Layers for Wearable Electronics and Optoelectronics. *ACS Appl. Mater. Interfaces* **2019**, *11* (12), 11061−11105.
(13) Lin, Y.; Gritsenko, D.; Liu, Q.; Lu, X.; Xu, J. Recent Advancements in Functionalized Paper-Based Electronics. *ACS Appl. Mater. Interfaces* **2016**, *8* (32), 20501−20515.
(14) Singh, E.; Meyyappan, M.; Nalwa, H. S. Flexible Graphene-Based Wearable Gas and Chemical Sensors. *ACS Appl. Mater. Interfaces* **2017**, *9* (40), 34544−34586.
(15) Weill, M.; Lutfalla, G.; Mogensen, K.; Chandre, F.; Berthomieu, A.; Berticat, C.; Pasteur, N.; Philips, A.; Fort, P.; Raymond, M. Comparative Genomics: Insecticide Resistance in Mosquito Vectors. *Nature* **2003**, *423* (6936), 136−137.
(16) Choi, M.; Park, Y. J.; Sharma, B. K.; Bae, S. R.; Kim, S. Y.; Ahn, J. H. Flexible Active-Matrix Organic Light-Emitting Diode Display Enabled by MoS2 Thin-Film Transistor. *Sci. Adv.* **2018**, *4* (4), 1−8.
(17) Yan, C.; Wang, J.; Lee, P. S. Stretchable Graphene Thermistor with Tunable Thermal Index. *ACS Nano* **2015**, *9* (2), 2130−2137.
(18) Xu, S.; Zhang, Y.; Jia, L.; Mathewson, K. E.; Jang, K. I.; Kim, J.; Fu, H.; Huang, X.; Chava, P.; Wang, R.; et al. Soft Microfluidic Assemblies of Sensors, Circuits, and Radios for the Skin. *Science* **2014**, *344* (6179), 70−74.
(19) Wang, Y.; Wang, L.; Yang, T.; Li, X.; Zang, X.; Zhu, M.; Wang, K.; Wu, D.; Zhu, H. Wearable and Highly Sensitive Graphene Strain Sensors for Human Motion Monitoring. *Adv. Funct. Mater.* **2014**, *24* (29), 4666−4670.
(20) Tran, T. X.; Choi, H.; Che, C. H.; Sul, J. H.; Kim, I. G.; Lee, S. M.; Kim, J. H.; In, J. B. Laser-Induced Reduction of Graphene Oxide by Intensity-Modulated Line Beam for Supercapacitor Applications. *ACS Appl. Mater. Interfaces* **2018**, *10* (46), 39777−39784.
(21) Wang, J. A.; Lu, Y. T.; Lin, S. C.; Wang, Y. S.; Ma, C. C. M.; Hu, C. C. Designing a Novel Polymer Electrolyte for Improving the Electrode/Electrolyte Interface in Flexible All-Solid-State Electrical Double-Layer Capacitors. *ACS Appl. Mater. Interfaces* **2018**, *10* (21), 17871−17882.
(22) Biswas, S.; Drzal, L. T. Multilayered Nano-Architecture of Variable Sized Graphene Nanosheets for Enhanced Supercapacitor Electrode Performance. *ACS Appl. Mater. Interfaces* **2010**, *2* (8), 2293−2300.
(23) Béguin, F.; Presser, V.; Balducci, A.; Frackowiak, E. Carbons and Electrolytes for Advanced Supercapacitors. *Adv. Mater.* **2014**, *26* (14), 2219−2251.
(24) Baughman, R. H.; Zakhidov, A. A.; De Heer, W. A. Carbon Nanotubes - The Route toward Applications. *Science* **2002**, *297* (5582), 787−792.
(25) Novoselov, K. S.; Fal'Ko, V. I.; Colombo, L.; Gellert, P. R.; Schwab, M. G.; Kim, K. A Roadmap for Graphene. *Nature* **2012**, *490* (7419), 192−200.
(26) Rinzler, A. G.; Liu, J.; Dai, H.; Nikolaev, P.; Huffman, C. B.; Rodriguez-Macías, F. J.; Boul, P. J.; Lu, A. H.; Heymann, D.; Colbert, D. T.; et al. Large-Scale Purification of Single-Wall Carbon Nanotubes: Process, Product, and Characterization. *Appl. Phys. A: Mater. Sci. Process.* **1998**, *67* (1), 29−37.
(27) Liu, T.; Finn, L.; Yu, M.; Wang, H.; Zhai, T.; Lu, X.; Tong, Y.; Li, Y. Polyaniline and Polypyrrole Pseudocapacitor Electrodes with Excellent Cycling Stability. *Nano Lett.* **2014**, *14* (5), 2522−2527.
(28) Zhang, Y.; Li, L.; Su, H.; Huang, W.; Dong, X. Binary Metal Oxide: Advanced Energy Storage Materials in Supercapacitors. *J. Mater. Chem. A* **2015**, *3* (1), 43−59.
(29) Long, J. W.; Swider, K. E.; Merzbacher, C. I.; Rolison, D. R. Voltammetric Characterization of Ruthenium Oxide-Based Aerogels and Other RuO2 Solids: The Nature of Capacitance in Nanostructured Materials. *Langmuir* **1999**, *15* (3), 780−784.

(30) Tao, F.; Zhao, Y. Q.; Zhang, G. Q.; Li, H. L. Electrochemical Characterization on Cobalt Sulfide for Electrochemical Supercapacitors. *Electrochem. Commun.* **2007**, *9* (6), 1282−1287.
(31) Liu, T. C.; Pell, W. G.; Conway, B. E.; Roberson, S. L. Behavior of Molybdenum Nitrides as Materials for Electrochemical Capacitors Comparison with Ruthenium Oxide. *J. Electrochem. Soc.* **1998**, *145* (6), 1882−1888.
(32) Wang, Y.; Yang, W.; Yang, J. A Co-Al Layered Double Hydroxides Nanosheets Thin-Film Electrode. *Electrochem. Solid-State Lett.* **2007**, *10* (10), 233−236.
(33) Han, Y.; Dai, L. Conducting Polymers for Flexible Supercapacitors. *Macromol. Chem. Phys.* **2019**, *220* (3), 1−14.
(34) Omastová, M.; Mičušík, M. Polypyrrole Coating of Inorganic and Organic Materials by Chemical Oxidative Polymerisation. *Chemical Papers* **2012**, *66* (5), 392−414.
(35) Shi, H.; Liu, C.; Jiang, Q.; Xu, J. Effective Approaches to Improve the Electrical Conductivity of PEDOT:PSS: A Review. *Adv. Electron. Mater.* **2015**, *1* (4), 1−16.
(36) Chani, M. T. S.; Karimov, K. S.; Khalid, F. A.; Moiz, S. A. Polyaniline Based Impedance Humidity Sensors. *Solid State Sci.* **2013**, *18* (12), 78−82.
(37) Goktas, H.; Wang, X.; Ugur, A.; Gleason, K. K. Water-Assisted Vapor Deposition of PEDOT Thin Film. *Macromol. Rapid Commun.* **2015**, *36* (13), 1283−1289.
(38) Skorenko, K. H.; Faucett, A. C.; Liu, J.; Ravvin, N. A.; Bernier, W. E.; Mativetsky, J. M.; Jones, W. E. Vapor Phase Polymerization and Mechanical Testing of Highly Electrically Conductive Poly(3,4-Ethylenedioxythiophene) for Flexible Devices. *Synth. Met.* **2015**, *209*, 297−303.
(39) Farka, D.; Coskun, H.; Gasiorowski, J.; Cobet, C.; Hingerl, K.; Uiberlacker, L. M.; Hild, S.; Greunz, T.; Stifter, D.; Sariciftci, N. S.; Menon, R.; Schoefberger, W.; Mardare, C. C.; Hassel, A. W.; Schwarzinger, C.; Scharber, M. C.; Stadler, P. Anderson-Localization and the Mott−Ioffe−Regel Limit in Glassy-Metallic PEDOT. *Adv. Electron. Mater.* **2017**, *3* (7), 1−8.
(40) Li, Y.; Hu, X.; Zhou, S.; Yang, L.; Yan, J.; Sun, C.; Chen, P. A Facile Process to Produce Highly Conductive Poly(3,4- Ethylenedioxythiophene) Films for ITO-Free Flexible OLED Devices. *J. Mater. Chem. C* **2014**, *2* (5), 916−924.
(41) Fabretto, M. V.; Evans, D. R.; Mueller, M.; Zuber, K.; Hojati-Talemi, P.; Short, R. D.; Wallace, G. G.; Murphy, P. J. Polymeric Material with Metal-like Conductivity for next Generation Organic Electronic Devices. *Chem. Mater.* **2012**, *24* (20), 3998−4003.
(42) Ouyang, J.; Chu, C. W.; Chen, F. C.; Xu, Q.; Yang, Y. Polymer Optoelectronic Devices with High-Conductivity Poly(3,4-Ethylenedioxythiophene) Anodes. *J. Macromol. Sci., Part A: Pure Appl.Chem.* **2004**, *41* (12), 1497−1511.
(43) Wang, X.; Zhang, X.; Sun, L.; Lee, D.; Lee, S.; Wang, M.; Zhao, J.; Shao-Horn, Y.; Dincă, M.; Palacios, T.; Gleason, K. K. High Electrical Conductivity and Carrier Mobility in OCVD PEDOT Thin Films by Engineered Crystallization and Acid Treatment. *Science Advances* **2018**, *4* (9), 1−10.
(44) Cho, B.; Park, K. S.; Baek, J.; Oh, H. S.; Koo Lee, Y. E.; Sung, M. M. Single-Crystal Poly(3,4-Ethylenedioxythiophene) Nanowires with Ultrahigh Conductivity. *Nano Lett.* **2014**, *14* (6), 3321−3327.
(45) D'Arcy, J. M.; El-Kady, M. F.; Khine, P. P.; Zhang, L.; Lee, S. H.; Davis, N. R.; Liu, D. S.; Yeung, M. T.; Kim, S. Y.; Turner, C. L.; et al. Vapor-Phase Polymerization of Nanofibrillar Poly(3,4- Ethylenedioxythiophene) for Supercapacitors. *ACS Nano* **2014**, *8* (2), 1500−1510.
(46) Zhang, Y.; Suslick, K. S. Synthesis of Poly(3,4-Ethylenedioxythiophene) Microspheres by Ultrasonic Spray Polymerization (USPo). *Chem. Mater.* **2015**, *27* (22), 7559−7563.
(47) Anothumakkool, B.; Soni, R.; Bhange, S. N.; Kurungot, S. Novel Scalable Synthesis of Highly Conducting and Robust PEDOT Paper for a High Performance Flexible Solid Supercapacitor. *Energy Environ. Sci.* **2015**, *8* (4), 1339−1347.
(48) Winther-Jensen, B.; West, K. Vapor-Phase Polymerization of 3,4-Ethylenedioxythiophene: A Route to Highly Conducting Polymer Surface Layers. *Macromolecules* **2004**, *37* (12), 4538−4543.
(49) Wanasekara, N. D.; Michud, A.; Zhu, C.; Rahatekar, S.; Sixta, H.; Eichhorn, S. J. Deformation Mechanisms in Ionic Liquid Spun Cellulose Fibers. *Polymer* **2016**, *99*, 222−230.
(50) Garreau, S.; Louarn, G.; Buisson, J. P.; Froyer, G.; Lefrant, S. In Situ Spectroelectrochemical Raman Studies of Poly(3,4-Ethylenedioxythiophene) (PEDT). *Macromolecules* **1999**, *32* (20), 6807−6812.
(51) Laforgue, A. All-Textile Flexible Supercapacitors Using Electrospun Poly(3,4- Ethylenedioxythiophene) Nanofibers. *J. Power Sources* **2011**, *196* (1), 559−564.
(52) Dai, Z.; Peng, C.; Chae, J. H.; Ng, K. C.; Chen, G. Z. Cell Voltage versus Electrode Potential Range in Aqueous Supercapacitors. *Sci. Rep.* **2015**, *5*, 9854.
(53) Jung, Y. H.; Chang, T. H.; Zhang, H.; Yao, C.; Zheng, Q.; Yang, V. W.; Mi, H.; Kim, M.; Cho, S. J.; Park, D. W.; et al. High-Performance Green Flexible Electronics Based on Biodegradable Cellulose Nanofibril Paper. *Nat. Commun.* **2015**, *6* (May), 1−11.
(54) Updegraff, D. M. Semimicro Determination of Cellulose Inbiological Materials. *Anal. Biochem.* **1969**, *32* (3), 420−424.
(55) Fathy, M.; Abdel Moghny, T.; Mousa, M. A.; El-Bellihi, A. H. A. A.; Awadallah, A. E. Absorption of Calcium Ions on Oxidized Graphene Sheets and Study Its Dynamic Behavior by Kinetic and Isothermal Models. *Appl. Nanosci.* **2016**, *6* (8), 1105−1117.
(56) Ghosh, S.; Remita, H.; Ramos, L.; Dazzi, A.; Deniset-Besseau, A.; Beaunier, P.; Goubard, F.; Aubert, P. H.; Brisset, F.; Remita, S. PEDOT Nanostructures Synthesized in Hexagonal Mesophases. *New J. Chem.* **2014**, *38* (3), 1106−1115.
(57) Slough, C. G. Weight Loss Determined from Mass Spectrometry Trend Data in a Thermogravimetric/Mass Spectrometer System. *Thermal Analysis Rheology*, pp 1−6.

https://dx.doi.org/10.1021/acsaem.9b02044
ACS Appl. Energy Mater. XXXX, XXX, XXX−XXX